The X-ray, optical and radio evolution of the GRB 030329 afterglow and the associated SN2003dh

R. Willingale, J.P. Osborne, P.T. O'Brien, M.J. Ward, A. Levan and K.L. Page
Department of Physics and Astronomy, University of Leicester, University Road, Leicester LE1 7RH

ABSTRACT

Extensive X-ray, optical and radio observations of the bright afterglow of the Gamma Ray Burst GRB 030329 are used to construct the multi-frequency evolution the event. The data are fitted using the standard fireball shock model to provide estimates of the initial energy, $\varepsilon = 6.8 \times 10^{52}$ ergs sr^{-1}, the density of the ambient medium, $n_0 = 1$ cm^{-3}, the electron and magnetic energy density fractions, $\epsilon_e = 0.24$ & $\epsilon_B = 0.0017$, the power law index of the relativistic electron spectrum, p = 2.25, and the opening angle of the jet, $\theta_j = 3$ degrees. Deviations from the standard model seen in the optical and radio are most likely attributable to the concurrent hypernova SN2003dh. Peaks at 0.23 and 1.7 days in the R-band are much brighter than expected from a standard SN, and there is a large radio excess over the expected afterglow flux for t>2 days. No deviation from the best-fit afterglow model is seen in the X-ray decline, indicating that the excess optical and radio flux from 1-5 days arises from a later injection of slower electrons by the central engine.

Key words: gamma-rays:bursts - shock waves - radiation mechanisms:non-thermal X-rays:general

1 INTRODUCTION

The trigger for GRB 030329 was made by HETE-II on 29 March 2003, 11:37:14.67 UT. Information promptly disseminated via the GRB Coordinates Network (GCN) by Vanderspek et al. (2003) prompted observations by a huge number of telescopes providing coverage in the X-ray, optical, IR, sub-millimetre and radio wavebands. The R band magnitude at 1.5 hours was 12.6 making it the brightest optical GRB afterglow seen at this epoch. The GRB lasted 25 seconds and had a peak flux of $\sim 7 \times 10^{-6}$ ergs cm^{-2} s^{-1} (30-400 keV) and a total fluence of $\sim 1.2 \times 10^{-4}$ ergs cm^{-2}, placing it in the top 0.2% of the observed fluence distribution. The redshift was determined as z=0.1685 by Greiner et al. (2003) and subsequently the isotropic energy released in the GRB has been estimated to be $E_{iso} \approx 9 \times 10^{51}$ ergs (30-400 keV) (Hjorth et al., Price et al., Uemura et al. 2003).

2 AFTERGLOW SPECTRUM OF A FIREBALL SHOCK

Here we summarise the continuum afterglow spectrum expected to arise from the standard fireball shock model (Mèszàros 2002 and references therein). An initial energy $E_{52} = E/10^{52}$ ergs is released very rapidly forming a fireball of e^+ e^- and gamma-rays which expands at extreme relativistic velocity (Lorentz factor Γ) into a surrounding medium of density n_0 forming a relativistic shock. A diminishingly small fraction of electrons is accelerated by repeated diffusion across the shock producing a power-law energy spectrum $N_e(\gamma_e) \propto \gamma_e^{-p}$. As the relativistic electrons spiral in the co-moving magnetic field we expect to see synchrotron radiation. A frequency ν_m is associated with the minimum electron energy $\gamma_{e,min}$ produced by the acceleration process. There will be some corresponding (very) high frequency ν^* associated with the maximum electron energy $\gamma_{e,max}$. A cooling-break frequency, ν_c, corresponds to the electron energy for which the synchrotron lifetime is comparable with the expansion time. The detailed form of the spectrum expected is described by Sari, Piran and Narayan (1998). At some early time t_0, $\nu_m = \nu_c$. For $t < t_0$ the electrons cool rapidly so that $\nu_m > \nu_c$ and for $t > t_0$ they cool slowly such that $\nu_m < \nu_c$. All the follow up observations of GRB 030329 fall into the latter regime. In the frequency range $\nu_m < \nu < \nu_c$ the spectrum, $F(\nu) \propto \nu^\beta$, has an index β directly related to the electron index p, $\beta = -(p-1)/2$. For $\nu > \nu_c$ the spectrum is steeper, $\beta \sim -p/2$. Below the peak, $\nu < \nu_m$, we expect $\beta \sim +1/3$ with the index increasing further to $\beta \sim +2$, at ν_a the self-absorption break, as the optical depth increases at low frequency.

Because the fireball is expanding relativistically with Lorentz factor Γ, the spectrum observed is blue-shifted. As the shock is arrested by the surrounding medium Γ decreases and the spectrum becomes redder. At early times we only see a small fraction of the radiating electrons because of rel-

Table 1. Temporal decay indices before t_0 and before and after the jet break t_j. Two sets of values are given for $t < t_0$, the first line for an adiabatic shock and the second line for the full radiative case. $F_m \propto t^{\alpha_f}$, $\nu_a \propto t^{\alpha_a}$, $\nu_m \propto t^{\alpha_m}$, $\nu_c \propto t^{\alpha_c}$.

	α_f	α_a	α_m	α_c
$t < t_0$ A	0	-1/2	-3/2	-1/2
$t < t_0$ R	-3/7	-4/5	-12/7	-2/7
$t < t_j$	0	0	-3/2	-1/2
$t > t_j$	-1	-1/5	-2	0

Table 2. Summary of X-ray observations of GRB 030329. The fluxes and spectral index β are for a photon energy of 1 keV.

	t days	Flux Jy	index β
RXTE	0.215	$(4.28 \pm 0.12) \times 10^{-5}$	-1.17 ± 0.04
RXTE	0.259	$(3.41 \pm 0.19) \times 10^{-5}$	-1.17 ± 0.04
RXTE	1.26	$(3.10 \pm 0.47) \times 10^{-6}$	-0.80 ± 0.3
XMM	37.3	$(5.74 \pm 0.35) \times 10^{-9}$	-1.08 ± 0.10
XMM	61.0	$(2.82 \pm 0.19) \times 10^{-9}$	-1.15 ± 0.12

Table 3. Power law decay indices before and after the break, and break times for the X-ray, optical and radio light curves of the afterglow. Error ranges are $\pm 1\sigma$ estimated from the least squares fitting procedure.

	α_0	α_1	t_b days
X-ray	-1.2 ± 0.1	-1.80 ± 0.06	0.57 ± 0.1
Optical	-0.87 ± 0.05	-1.84 ± 0.07	0.52 ± 0.05
Radio	$+0.89 \pm 0.08$	-0.55 ± 0.10	9.86 ± 0.06

ativistic beaming and only a small fraction of the expanding shock is visible. As Γ decreases the relativistic beaming angle opens up and if the expansion is isotropic the observed flux at the peak, F_m, remains constant while the frequency of the peak changes as a power-law, $\nu_m \propto t^{-3/2}$. The self-absorption break, ν_a, remains constant but the cooling break also varies as a power law, $\nu_c \propto t^{-1/2}$. Wijers & Galama (1999) provide full expressions for the expected synchrotron spectrum parameters in terms of energy per steradian $\varepsilon_{52} = E_{52}/4\pi$, ambient interstellar density n_0 cm^{-3}, X the hydrogen mass fraction of the ambient medium, p the electron power-law index, χ_p and ϕ_p the dimensionless peak location and peak flux which are functions of p, ϵ_e the electron energy fraction (wrt the energy density of nucleons), ϵ_B the magnetic energy density fraction (again wrt the energy density of nucleons), the redshift z of the GRB and finally $h_{70} = H_0/70$ km s^{-1} Mpc^{-1}.

If the relativistic outflow is collimated in a jet with open angle θ_j then the evolution of the spectrum is modified (Rhoads 1997, 1999; Sari, Piran & Halpern 1999; Frail et al. 2001; Panaitescu & Kumar 2001b). At time t_j, when $\Gamma^{-1} \approx \theta_j$, we expect to see an achromatic break in the decay of the afterglow because we can see the edge of the jet structure and because the material has time to expand sideways. After the break the decay of the peak flux, peak frequency, the cooling break and the self-absorption break are modified, $F_m \propto t^{-1}$, $\nu_m \propto t^{-2}$, $\nu_c = const.$ and $\nu_a \propto t^{-1/5}$. The details of the changes in the decay indices depends on the density profile of the surrounding medium and the time dependence of the jet spreading assumed. The energy losses of the emitting electrons and the observed spectral form is also expected to be modified by inverse Compton scattering (Panaitescu & Kumar 2001a, Sari & Esin 2001).

If $F_m \propto t^{\alpha_f}$, $\nu_m \propto t^{\alpha_m}$ and $F(\nu) \propto \nu^{\beta_0}$ then the flux at a frequency $\nu_m < \nu < \nu_c$ has a temporal variation given by:

$$F_\nu \propto t^{\alpha_f - \alpha_m \beta_0} \tag{1}$$

If $\nu_c \propto t^{\alpha_c}$ then for frequencies $\nu > \nu_c$ the spectral form is $F(\nu) \propto \nu^{\beta_1}$ and the temporal variation is $F_\nu \propto t^{\alpha_f - \alpha_m \beta_0 - \alpha_c(\beta_1 - \beta_0)}$. The change in spectral index across the cooling break is $\beta_1 - \beta_0 = -p/2 + (p-1)/2 = -1/2$ so at frequencies above the cooling break we have:

$$F_\nu \propto t^{\alpha_f - \alpha_m \beta_0 + \alpha_c/2} \tag{2}$$

Table 1 lists the temporal indices of the peak flux and break frequencies expected before t_0 and before and after the jet break (Sari, Piran & Halpern 1999).

3 MULTI-FREQUENCY DATA

To calculate a reliable estimate of the physical parameters of a GRB afterglow under the fireball shock model we must measure F_m, ν_m, ν_c and ν_a. However, this is not easy to do directly. Most studies of GRB afterglows to date have concentrated on the interpretation of light curves in a single waveband, in some cases augmented by sparse multi-frequency data. Much attention has been given to the study of decay breaks in light curves. These may correspond to a jet break (if achromatic) or a spectral break passing through a given pass band as the afterglow reddens. In order to extrapolate the decay behaviour in a single waveband we must have a reliable model for the decay, especially after a jet break when the details depend on the structure of the surrounding medium and the expansion at the edge of the jet.

The afterglow of GRB 030329 was particularly bright and has therefore been subjected to extensive temporal and spectral observational coverage. We have gathered together published photometric data from the afterglow in the radio, sub-millimetre, IR, optical and X-ray energy bands. We have re-analysed the data from the XMM observations yielding flux and spectral index estimates consistent with Tiengo et al. 2003c. Table 2 summarises all the X-ray measurements with the fluxes quoted in Jy at 1 keV. The RXTE results are taken from Tiengo et al. (2003c). The optical fluxes were calculated assuming a Galactic reddening correction of E(B-V)=0.025 mag. (Burenin et al. 2003b, Matheson et al. 2003).

Fig. 1 shows the evolution of the afterglow in the three main energy bands. We have performed a multi-frequency fit using the fireball shock model in a similar manner to Harrison et al. (2001), Panaitescu & Kumar (2001a,2002,2003), Frail et al. (2003) and Yost et al. (2003). The coverage of the present data for GRB 030329 is much greater in time and frequency than for any previous burst and therefore the fitting is constrained at a far higher level. The solid lines in Fig. 1 show the best fit afterglow model which is described in detail below. A clear temporal break is seen in the decay curves of each waveband. Table 3 lists the decay indices before (α_0) and after (α_1) the break time (t_b) estimated using simple power-law fits. The optical light curve suffers an
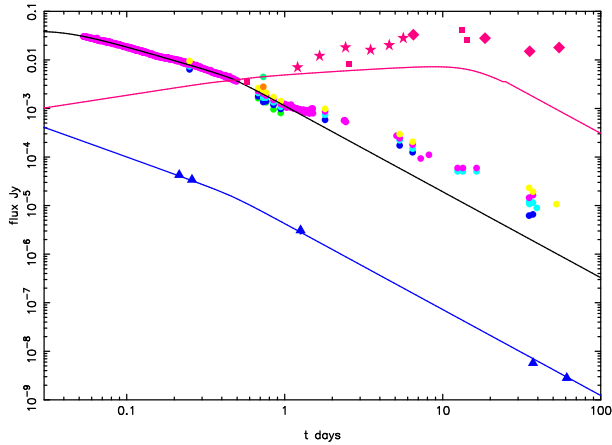
Figure 1. The afterglow flux in X-rays (1.0 keV plotted in blue), optical (V, B, R and I plotted respectively as blue, green, red and yellow dots) and radio (7.7 GHz diamond, 8.5 GHz square and 15.2 GHz star plotted in red). The curves show the best fit model in X-ray (1 keV), optical (R-band) and radio (8.5 GHz). Data sources (all 2003): X-ray - Marshall and Swank; Marshall, Markwardt and Swank; Tiengo et al.; Optical/IR - Bikmaev et al.; Burenin et al.; Fitzgerald and Orosz; Gorosabel et al.; Ibrahimov et al.; Lamb et al.; Lee et al.; Price et al.; Simoncelli et al.; Stanek et al.; Susuki et al.; Testa et al.; Uemura et al.; Zharikov et al.; Sub-millimetre - Hoge et al.; Radio - Berger et al.; Bloom et al.; Finkelstein et al.; Kuno et al.; Pooley; Rao et al.; Trushkin et al.
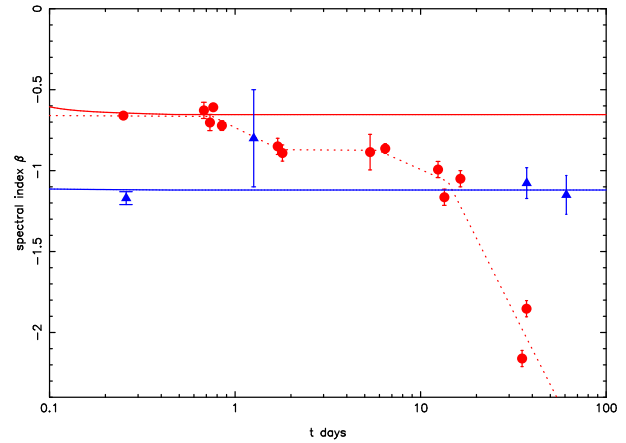

Figure 2. The spectral indices of the afterglow in X-rays (1.0 keV plotted as blue triangles) and optical (plotted as red circles). The solid lines show the evolution of the spectral index of the optical and X-ray in the best fit model of the afterglow component. The dotted line indicates the observed evolution of the optical spectral index. Note that the earliest X-ray point is derived from the combination of the first two RXTE observations (see Table 2). Data sources (all 2003): X-ray - Marshall and Swank; Marshall, Markwardt and Swank; Tiengo et al.; Optical - Burenin et al.; Fitzgerald and Orosz; Ibrahimov et al.; Lamb et al.; Lee et al.; Simoncelli et al.; Testa et al.; Zharikov et al.

initial break at ~ 0.5 days steepening to $\alpha_1 = -1.84$ as indicated in Table 3 but at ~ 1 day it flattens off to $\alpha_2 = -0.73$, finally turning over again at ~ 3 days to $\alpha_3 = -1.35$.

Optical spectroscopy indicates that between 1 and 10 days an optical SN was emerging from the baseline afterglow of the GRB (Stanek et al. 2003b). Fig. 2 shows the measured values of the optical and X-ray spectral indices. The optical BVRI index is $\beta_0 = 0.66 \pm 0.01$ at 0.25 days (Burenin et al. 2003b) and gradually reddens for $t > 1.0$ days as the SN component starts to dominate. The evolution of the optical spectrum is analysed in greater detail by Matheson et al. (2003). Their data and analysis confirm the gradual change in spectral index for $1 < t < 5$ days followed by a more dramatic change for $t > 6$ days as shown in Fig. 2. The weighted mean of the four X-ray measurements is $\beta_X = 1.13 \pm 0.06$. The solid lines are the predicted indices from the best fit afterglow model (see below) and the dotted line indicates the gradual change of the optical index which starts at ~ 1 day.

The difference between the optical and X-ray spectral indices for $t < 1.0$ days is -0.47 ± 0.06 consistent with the expected change across the cooling break frequency, ν_c, $\beta_1 - \beta_0 = -0.5$. Before $t_b = 0.57$ days in the X-ray light curve the temporal index is $\alpha_0 = -1.2 \pm 0.1$ which is consistent with the expected value before the jet break of $-\alpha_m \beta_0 + \alpha_c = -1.3$ calculated using equation 2 if $\beta_0 = 0.7$. Similarly the optical temporal index $\alpha_0 = -0.87 \pm 0.05$ is consistent with the expected value $-\alpha_m \beta_0 = -1.0$ from equation 1. The slightly low optical value probably arises because the curvature of the afterglow spectrum produces a smaller value of β_0 near the peak. The temporal decay indices of the X-ray and optical light curves immediately after t_b are very similar, $\alpha_1 \sim -1.8$. If we interpret t_b as the jet break t_j we can use equations 1 and 2 to predict $\alpha_1 = -2.4$ for both

X-rays ($\nu > \nu_c$) and optical ($\nu < \nu_c$) since $\alpha_c = 0$ for $t > t_j$. Although the X-ray and optical light curves are decaying at the same rate this rate is somewhat less than expected for $t > t_j$. This maybe because $\alpha_f \sim 0.5$ (see below) rather than $\alpha_f \sim -1.0$, as listed in Table 1, or α_m did not change from $-3/2$ to -2 as expected.

The optical data for $t < 0.1$ days and $0.6 < t < 1.0$ days, the earliest 8.46 GHz measurement (Berger et al. 2003a), the earliest 1.288 GHz measurement (Rao et al. 2003a,b) and all the X-ray data were fitted using a χ^2 statistic constructed from $\log F(\nu, t)$ and the expected fireball shock spectrum including a jet break. The X-ray data are particularly important because they cover a wide temporal window and are not expected to include flux from any supernova component or the host galaxy. The radio and optical data for $t > 1.0$ days were excluded from the fit because the rise in these two wavebands was probably augmented by flux from the detected SN. The optical data in the range 0.1-0.6 days were excluded because an optical bump in this range resulted in a higher χ^2 value. This small optical bump is noticeable in the original plot of the optical data presented by Uemura et al. (2003). A total of 207 data points gave $\chi^2 = 275$. With 8 free parameters in the model there were 199 degrees of freedom and the $\chi^2_\nu = 1.38$. If the optical data in the range 0.1-0.6 days were included the reduced Chi-squared increased, $\chi^2_\nu = 2.64$. The best fit parameter values and estimated 90% confidence limits are given in Table 4. These parameter values are not significantly changed if we include the optical data 0.1-0.6 days. It is remarkable the standard fireball shock model is a good fit for all wavebands (X-ray, optical and radio) for $t < 1$ day and the agreement continues up to $t \sim 60$ days in X-rays. Furthermore the model provides an excellent fit to the measured spectral indices in the optical ($t < 1$ day) and X-rays as indicated in Fig. 2.

The n_{sm} parameter was used to smooth the broken

Table 4. Best fit parameter values and 90% confidence limits for the parameters of fireball shock spectral model at $t = 0.2$ days

Fm Jy	0.0521	0.0507-0.0537
ν_a Hz	7.4×10^9	$(5.3 - 10) \times 10^9$
ν_m Hz	3.3×10^{13}	$(3.1 - 3.5) \times 10^{13}$
ν_c Hz	1.3×10^{16}	$(0.9 - 1.8) \times 10^{16}$
p	2.25	2.24-2.26
t_j days	0.47	0.42-0.51
α_f	-0.48	-(0.43-0.54)
n_{sm}	2.1	1.8-2.5

power-law sections in the way described by Beuermann et al. (1999). This produces the curvature required to fit the early optical light curve and is responsible for the slight rise in the optical spectral index at early epochs as shown in Fig. 2. Explicitly, the model spectrum consists of four power-law sections combined using a smoothing parameter:

$$F(\nu, t) = (F_0^{-n_{sm}} + F_1^{-n_{sm}} + F_2^{-n_{sm}} + F_3^{-n_{sm}})^{-1/n_{sm}} \quad (3)$$

where $F_i = k_i \nu^{\beta_i}$. The breaks between the sections occur at ν_a, ν_m, ν_c which evolve with t as indicated in Table 1. The order of the break frequencies depends on t because they evolve at different rates. The power-law indices for $t > t_0$ are given in section 2. If the model is used for $t < t_0$ then we set $\beta_2 = -1/2$ but this does not effect the data fitting and only applies when the model is used at very early times. The normalisations k_i are calculated to give a continuous curve with a peak value F_m (before smoothing). The effect of the smoothing is only seen close to the breaks as indicated in the model curves plotted in Fig. 4.

The temporal decay index of F_m after the jet break, $\alpha_f = -0.48$, is determined by the last three X-ray data points and the optical measurements $0.6 < t < 1.0$ days. This result is consistent with the analysis presented by Tiengo et al. (2003c) but identifies the X-ray temporal decay index $\alpha_1 = -1.8$ with the decay in the peak flux of the fireball spectrum. Fig. 3 shows the residuals about the peak flux (F_m) of the best fit model. The last three X-ray data values clearly define the peak decline after the jet break. Fig. 3 also includes the optical data for $0.1 < t < 0.6$ and $t > 1.0$ which were excluded from the fitting procedure. The faint optical bump with a peak at ≈ 0.25 days and the dramatic rise in the optical flux just after $t = 1.0$ day are apparent. Figure 4 shows a series of four snap shots of the evolution of the spectrum. In the lower panels at 1.26 and 2.5 days the optical and higher frequency radio measurements are starting to lift away from the underlying afterglow component. The absorption break ν_a is the least constrained parameter because it is only determined by the radio measurements included at 0.63 and 2.5 days. All plots cover a flux range of 10^{-7} to 0.1 Jansky and 3×10^8 to 10^{18} Hz. We attempted to find an acceptable fit including the later optical and radio data. It was possible to get a fit without including a jet break but this predicted an X-ray flux a factor of ~ 20 greater than observed for $t > 30$ days and a factor of ~ 3 smaller than the observed for $t < 1$ day and, furthermore, the residuals for the optical data over the period $0.5 < t < 3.0$ days were unacceptably large. At the same time the radio measurements were poorly represented. In particular the mean flux densities at 3.9, 7.7 and 11.2 GHz from Trushkin et al. (2003)
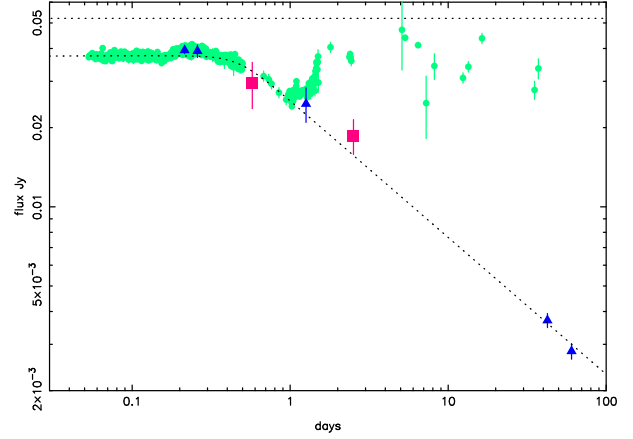

Figure 3. Residuals about peak flux of the best fit afterglow. Because we performed the fitting in log $F(\nu, t)$ the difference between data and the model (calculated at the observed frequency) is naturally expressed as a ratio. This ratio is shown multiplied by the peak flux of the model (F_m) so that the jet break in the model is apparent. The horizontal dotted line indicates the peak flux expected without smoothing or the jet break. The dotted curve is the peak flux with smoothing and including the jet break. Optical R-band plotted as circles, Radio (7.7, 8.5 and 15.2 GHz) squares, X-ray (1 keV) triangles.
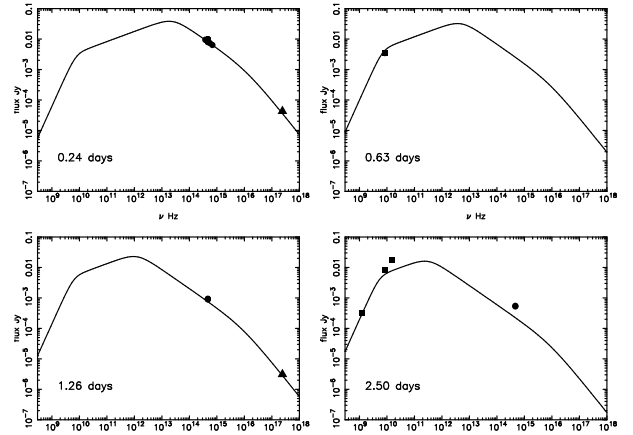

Figure 4. The evolution of the broadband spectrum. The best fit continuum is shown as a curve. The measured points are X-ray (triangles), optical (circles) and radio (squares). Error bars were plotted but they are too small to be seen at this scale. The lowest frequency radio data point (1.288 GHz) in the bottom right panel is taken from Rao et al. (2003a,b) and constrains the ν_a value in the model.

gave spectral indices which contradict the expected trend. Scintillation is expected to introduce variability in the observed radio fluxes. For the Galactic coordinates $l_{II} = 217$, $b_{II} = +60.7$ of GRB 030329 the rms variability expected at 8.5 GHz is $\sim 30\%$ with a time scale of a few hours (Walker 1998) consistent with the errors used at this frequency. The variability will be larger at 1.288 GHz but the flux used in the fitting from Rao et al. (2003a,b) for 31 March 2003 is the average from 8 hours observation with 2-sigma error bars. We conclude that the best fit of the afterglow model is not susceptible to scintillation.

Figure 5 shows the residual optical and radio flux seen over and above the best fit fireball shock model. The model
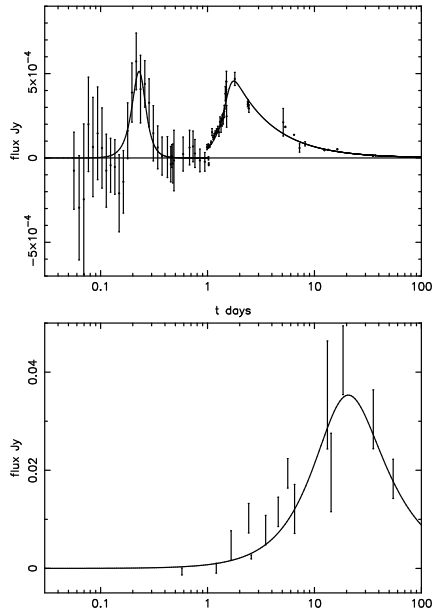
Figure 5. The residual optical (R-Band) and radio flux (7.7, 8.5 and 15.2 GHz) after subtracting the best fit fireball shock model. The early optical data points ($t < 2.0$ days) have been binned to improve the statistics. The radio fluxes have not been corrected to a nominal frequency. The curves are simple power-law fits to the rise and fall of each peak. The first two radio data points (at 8.46 GHz) are consistent with the standard fireball model.

Table 5. Physical parameters derived from the best fit afterglow model together with 90% confidence ranges.

ε_{52}	6.8	5.1-9.0
n_0 cm^{-3}	1.0	0.26-4.1
ϵ_e	0.24	0.18-0.31
ϵ_B	0.0017	0.0007-0.0038
p	2.25	2.24-2.26
θ_j degrees	3.0	2.4-3.9
E_{50} (ergs in jet)	1.9	1.7-2.1

is an excellent fit to the optical data $t < 0.2$ days and $0.6 < t < 1.0$ days and the very early radio points. However there is highly significant additional flux seen in both the radio and optical which does not fit the standard model (see also Tiengo et al. 2003c).

4 PHYSICAL PARAMETERS

We have used the formulation of Wijers & Galama (1999) to calculate the physical parameters of the afterglow. We assumed a hydrogen mass fraction $X = 0.7$ and used the $p = 2.25$ value to estimate $\phi_p = 0.62$ and $\chi_p = 0.56$ on the plots provided by Wijers & Galama (1999). The results are listed in Table 5. The θ_j and E_{50} values were derived from the formula given by Sari, Piran and Halpern (1999) which specifies the jet break as the time when lateral adiabatic expansion of the jet becomes apparent. The ranges of physical parameters given in Table 5 were estimated from the 90% confidence ranges of the fit parameters given in Table 4. In fact the ranges are dominated by the uncertainty in ν_a.

The index $\alpha_f = -0.48$ for the temporal evolution of F_m for $t > t_j$ is the only afterglow parameter which does not conform to the standard model. If the expansion after the jet break is adiabatic the we expect $\alpha_f \sim -1$. This result suggests that either the edge of the jet is not well defined (the jet has a broad smooth profile rather than a sharp edge, Panaitescu & Kumar 2003) or something is confining the expected expansion.

Using the afterglow model we can extrapolate back to the epoch of the GRB. From the best fit values of ν_m and ν_c we find $t_0 = 5 \times 10^{-4}$ days (43 seconds) which is only ~ 18 secs after the burst faded. Using the full radiative evolution values for $t < t_0$ from Table 1 we get a total fluence in the 25 second burst of 1.1×10^{-4} ergs cm^{-2} which is remarkably close to the measured estimate of 1.2×10^{-4} ergs cm^{-2}. The F_m value must have remained constant from 25 seconds to the break at 0.47 days as expected from the standard model. The afterglow model gives $\varepsilon \approx 6.8 \times 10^{52}$ ergs per steradian for the shock, while the fluence from the GRB was $\varepsilon_{52\gamma} \approx 0.07$. Hence we estimate that $\sim 1\%$ of the explosion energy was radiated as γ-rays in the GRB.

The spectral analysis used to derive the physical parameters in Table 5 assumes that the afterglow spectrum is dominated by synchrotron emission, ignoring any contribution from self-Compton emission from the relativistic shock. Inverse Compton (IC) scattering is expected to modify the high-energy tail of the spectrum producing a characteristic bump in the X-ray and γ-ray energy bands. Using the formulation of Sari & Esin (2001) we can use the physical shock parameters in Table 5 to estimate the photon energy at which the synchrotron and IC component fluxes are the same. The result is > 50 keV for all epochs. Therefore the bulk of any IC emission is expected to be above the RXTE and XMM energy band and hence unobserved. IC cooling is expected to be important at early times in the afterglow evolution even if it is not observed directly. In the fast cooling stages IC scattering increases the radiation losses by a factor $\sim (\epsilon_e/\epsilon_B)^{1/2} \approx 12$ thereby delaying the transition to the slow cooling regime to $t_0 \approx 0.15$ hours. However this is still well before the first optical observations of GRB 030329 were made. IC cooling continues to be important for $t > t_0$ while the fireball (or jet) is relativistic. After the system has proceeded through the jet break and ceases to be highly relativistic the efficiency of IC cooling drops rapidly and ceases to be important. Since we observe a break which is probably the jet break at $t \approx 0.5$ days we can be confident that our results are not compromised by IC emission.

5 ORIGIN OF THE EXCESS FLUX

There are two optical bumps in the residuals plot Fig. 5. The solid lines in the plots are simple power fits used to estimate the peak positions and integrated fluxes. The first R-band peak has a maximum at 0.23 days, a FWHM of 0.06 days (5% peak flux range 0.14 to 0.35 days), and an integrated flux of 5.5 Jy secs corresponding to a total energy of $\approx 1.4 \times 10^{48}$ ergs in the optical waveband ($\Delta\nu \approx 4 \times 10^{14}$ Hz). The rise time is only ~ 0.09 days and the maximum flux is $\sim 6 \times 10^{-4}$ Jy corresponding to $R_{mag} \approx 16.8$. The second R-band peak is a much longer. It has a maximum at 1.7 days, a FWHM of 2.0 days (5% peak flux range 0.9 to ~ 28

Table 6. Properties of the flux peaks in excess of the best fit afterglow model.

	first R-band	second R-band	radio ~ 8 GHz
t_{start} days	0.14	0.9	1.0
t_{max} days	0.23	1.7	20
t_{end} days	0.35	~ 28	> 100
FWHM days	0.06	2.0	~ 38
rise time days	0.09	0.8	~ 17
peak flux Jy	6×10^{-4}	4.5×10^{-4}	0.035
peak R_{mag}	16.8	17.1	-
optical ergs	$\sim 1.4 \times 10^{48}$	$\sim 5.9 \times 10^{49}$	-

days), and an integrated flux of 234 Jy secs corresponding to a total of $\approx 5.9 \times 10^{49}$ ergs in the optical waveband. Again, the rise time of ~ 0.8 days is remarkably short, the maximum flux is $\sim 4.5 \times 10^{-4}$ Jy corresponding to $R_{mag} \approx 17.1$. It is interesting that the spectral index of the optical spectrum starts to redden at ~ 1 day (see Fig. 2) at the onset of this second R-band peak. Although the maximum flux for the two optical peaks is similar, because the afterglow is decaying rapidly the first R-band peak represents only a small increase over and above the underlying afterglow, $\sim 5\%$, while the second peak corresponds to a large increase of $\sim 100\%$.

A single broad radio peak (7.7, 8.5 and 15.2 GHz data points) is also shown plotted in Fig. 5. It has a maximum of ~ 0.035 Jy (at ~ 8 GHz) at ~ 20 days corresponding to the time of emergence of the full SN spectrum, Hjorth et al. (2003). The peak luminosity is $\sim 3 \times 10^{31}$ ergs s^{-1} Hz^{-1}. The properties of the first and second R-band peaks and the radio peak are summarised in Table 6.

There are a number of possible explanations for the excess flux seen over and above the standard fireball shock. We will discuss them under three headings; Afterglow effects - modifications to the standard afterglow shock model; Dust echoes - scattering of afterglow radiation back into our line of sight; SN/Hypernova - optical and radio flux from a stellar explosion. A key feature of the observed residuals is that they are not seen in X-rays and they are not the same in the optical and radio. The first R-band peak is a short flash while the second R-band peak is a longer outburst and the radio peak reaches a maximum at a much later time than the second R-band peak.

5.1 Afterglow effects

If the ISM about the progenitor were inhomogeneous (varying density n_0) then we might expect to see rapid and noticeable deviations from a smooth power-law decay. Such an effect was considered by Wang & Loeb (2000) and has been used to explain variations seen in several afterglows (e.g. GRB 011211, Holland et al, 2002; Jakobsson et al, 2003; GRB 021004, Lazzati et al, 2003; Holland et al, 2003). For $t < t_j$ (Nakar, Piran and Granot 2003) and below the cooling break ($\nu < \nu_c$, usually the optical regime) the flux is expected to be $F_\nu \propto n^{(p+1)/4}$ whilst for $\nu > \nu_c$ (the X-ray regime) the flux is only weakly dependent on density. Therefore the first peak in the R-band flux, which corresponds to a very modest increase $\Delta F_\nu \sim 5\%$, could easily be due to a small increase in ambient density. However, for $t > t_j$ the

opposite is true (Nakar, Piran and Granot 2002). Here we expect a change in density to increase the X-ray flux more than the optical. It is therefore most unlikely that the second R-band peak, which corresponds to an increase of the optical afterglow flux by $\sim 100\%$ and is not accompanied by a similar large increase in the X-ray flux, is caused by a rise in ambient density.

Refreshed shocks due to sustained activity in the central engine have been used to explain the observed lightcurve of GRB 021004, which was unusually flat for the first few hours, and shows correlated X-ray and optical changes (Fox et al., 2003). This model has also been invoked for GRB 030329 (Granot, Nakar and Piran 2003). Refreshed shocks should be seen as correlated outbursts in the X-ray and optical decays although the fractional increase seen in optical and X-ray is not expected to be the same (Sari & Mèszàros 2000). At the same time we might also expect to see a change in the X-ray and optical spectra. Because of the sparse X-ray coverage we cannot rule out the possibility that the optical excess arises from refreshed shocks and any associated small increase in the X-ray flux was unfortunately missed. However, the fit of the standard model to the available X-ray data is very good and we see no change in X-ray spectral index. We think it is unlikely that all the excess optical flux arises from refreshed shocks. There is variability in the excess flux of the second peak and at least three more re-brightenings were identified by Granot, Nakar and Piran (2003) at $t \sim 2.6$ days, $t \sim 3.3$ days and $t \sim 5.3$ days. They favour refreshed shocks as the most likely explanation for these features. However, analysis of millimeter observations presented by Sheth et al. (2003) shows that there is no short-lived millimeter emission associated with bumps in the optical light curve indicating that central engine of the GRB was not injecting energy on these timescales.

A further possibility is that we are observing lateral structure within the jet rather than axial structure imposed by the ambient medium. This possibility is investigated by Granot & Kumar (2003), Kumar & Granot (2003) and Salmonson (2003). However such structure is expected to modify the overall evolution of the light curve producing, for example, a late temporal break in the afterglow decay and is not expected to produce rapid variations or bursts.

We conclude that at least the second optical bump is not due to afterglow effects.

5.2 Dust Echoes and Scattering

Dust echos were considered to be a possible explanation of late time bumps in the light curves of some GRBs (Waxman & Draine, 2000). In this scenario dust close to the burst is sublimed by the prompt X-ray and EUV radiation, whilst dust beyond the sublimation radius absorbs the energy and then re-radiates it at longer wavelengths. Bumps or flares are expected to occur at late times after the GRB (the the exact times being a function of the sublimation radius of the burst, and of course the assumed beaming geometry). Because dust sublimes at ~ 2000K the bumps are necessarily very red and are unlikely to have significant flux in the optical band. We do not consider them a viable explanation of the bumps in GRB 030329.

Esin & Blandford (2000), and subsequently Reichart (2001), take a different approach in which the scattering of

the initial optical flash by the dust is responsible for a bump in the afterglow light curve. Reichart (2001) finds that for values of $\theta_j \leq 5$ degrees, and small sublimation radii the echo can reach maximum in less than one day, consistent with the first R-band peak. If the efficiency of the reflection/scattering process is ~ 0.1 it is unlikely that these models can explain the second R-band peak which has a very large integrated energy implying a huge initial burst.

5.3 SN/Hypernova

At $z = 0.1685$ GRB 030329 provides a unique opportunity to probe the early behaviour of any associated SN. There is overwhelming evidence that the spectroscopic signature of a SN Type Ic forms part of the optical afterglow of GRB 030329 (Hjorth et al. 2003). This supernova has been designated SN2003dh (Stanek et al. 2003a, Garnavich et al. 2003). The expansion velocity measured at 10 days was $36,000 \pm 3,000$ km s^{-1}, larger than any previously know SN and it is therefore worthy of the title hypernova. Crude spectroscopic dating concludes that the SN was coincident with GRB 030329 ± 2 days (Hjorth et al. 2003). Using the spectroscopic evidence alone Matheson et al. (2003) conclude that SN2003dh emerges at $t > 6$ days. The photometric evidence (after subtraction of the standard afterglow component) and the onset of the changes in optical spectrum for $t > 1.0$ days (see Fig. 2) indicate that the optical flux associated with SN2003dh is detected earlier than this.

Any premaximum display of variability in the SN lightcurve including the shock breakout and structure introduced as the shock propagates through the layered structure of the star may be visible. Indeed, the short first R-band peak followed by the extended second R-band peak shown in Fig. 5 are very similar to the model light curves of Type Ib SN models shown by Ensman & Woosley (1998), although the time scale is a factor of 6-10 faster. Models of Type Ic SNe by Nakamura et al. (2001) indicate that the peak of the luminosity for such events should occur in the range 10-15 days. The peak of the main outburst in Fig. 5 is at $t \approx 1.7$ days, much earlier than predicted from the models. SN1998bw peaked at $M_V = -19.35$, $M_R = -19.36$ (Galama et al. 1998). Scaling this to z=0.1685 gives $R_{mag} = 20.22$, therefore the peak of the long optical outburst in Fig. 5 $R_{mag} = 17.1$ is ~ 18 times brighter than SN1998bw, having $M_V \approx -22.5$.

The SN 1b models of Ensman & Woosley (1988) produce a main peak FWHM of 25 days as observed for SN1983N (the only event for which good data are available), which is only possible for the lower mass models (Wolf-Rayet = 4-6 M$_\odot$, orig mass = 15-20 M$_\odot$). More massive models create broader peaks, as do less powerful explosions. A smaller ejected mass gives a lower duration because the radioactive luminosity diffuses out quicker. However a small ejected mass results in a dim SN since it is powered by the ejected Ni. In modelling SN 1998bw Nakamura et al. (2001) show that the main peak width is proportional to the ejected mass $M_{ej}^{3/4}$ and the explosion energy $E^{-1/4}$, while the velocities scale as $M_{ej}^{-1/2}$ and $E^{1/2}$. These relationships point to either a low ejected mass or a high powered explosion in GRB 030329 or both. The FWHM of 1998bw was ~ 29 days and the ejection velocity at 10 days is $\sim 26,000$ km

s^{-1}. This is fit with $E = 5 \times 10^{52}$ ergs and $M_{ej} = 10$ M$_\odot$ by Nakamura et al. (2001). Scaling from this we estimate the energy and mass of SN2003dh as $E = 5 \times 10^{51}$ ergs and $M_{ej} = 0.6$ M$_\odot$. This is a significantly lower ejected mass than considered by Ensman & Woosley (their values were based on there being a He envelope present).

Sheth et al. (2003) and Berger et al. (2003b) suggest that the observed excess radio and millimeter flux (and by implication excess optical flux) from GRB 030329 arises from a second slower and wider jet-like outflow. The shock in such an outflow would generate a spectrum similar to the standard model illustrated in Fig. 4 but with the absorption break and peak shifted to much lower frequencies. This could account for the broad radio and optical excess but would not generate a significant X-ray flux, consistent with the analysis presented above. It might also explain the change in the optical spectral index which starts at t=1 day. However it would not account for the very fast optical flux increase seen at the onset of the second optical peak. This would require a large extra injection of energy at t=1 day, similar in kind to a refreshed shock, rather than a slower, wider outflow launched at t=0. The duration and timing of the radio peak are very similar to known RSNe. However, the peak luminosity of $\sim 3 \times 10^{31}$ ergs s^{-1} Hz^{-1} is a factor of 10^4 higher than typical Type Ib/c RSNe (Weiler et al. 2002) but very similar to the radio afterglows seen for GRB 991208, $\sim 2 \times 10^{31}$ ergs s^{-1} Hz^{-1}, and for GRB 970508, $\sim 9 \times 10^{30}$ ergs s^{-1} Hz^{-1} (Frail, Waxman & Kulkarni 2000) at 5 GHz. This, again, clearly indicates that the hypernova in GRB 030329 was indeed a powerful event.

The combination of a rapid first peak and a very bright second peak is not predicted by standard models of SNe. The second peak is too bright and reaches peak too quickly to be entirely fuelled by the radioactive decay of a large mass of ^{56}Ni (Woosley & Heger 2003). If the excess flux is directly associated with the hypernova then it arises from the injection of energy from some other source. Both the optical and radio maxima were very bright compared with previously observed SNe/hypernovae. This may be due to the geometry of the explosion rather than just a very large explosion energy. The ejecta could be beamed and/or the visible envelope of the expanding photosphere might be flattened. Since the hypernova was concurrent with a GRB this seems reasonable although we know of no detailed models which address such a scenario.

6 CONCLUSION

The high quality and extensive coverage of data available from GRB 030329 has enabled us to calculate the physical parameters of the event with high precision and has revealed important details about the concurrent hypernova SN2003dh.

The GRB released an energy of $\sim 1.9 \times 10^{50}$ ergs into a jet with open angle ~ 3 degrees and about 1% of this energy was radiated away as γ rays. The jet propagated in a medium with $n_0 = 1$ cm^{-3} and the shock generated an relativistic electron spectrum with index $p = 2.25$. The electron and magnetic field energy densities in the shock were $\epsilon_e = 0.24$ and $\epsilon_B = 0.002$. A jet break occurred at 0.5 days after which the peak flux of the afterglow, F_m, decayed with $\alpha_f = -0.5$.

It is likely that the lightcurves shown in Fig. 5 are directly associated with the hypernova SN2003dh. This event had the spectroscopic signature of a SN 1c by 8-10 days but the fast rise and decline in the optical, the very bright optical peak and the large radio excess are not standard SN 1c properties. The excess optical and radio flux probably arise from an afterglow powered by a central engine such as the disk wind component proposed by Woosley & Heger (2003) but injection of energy at $t \approx 1$ day is required to explain the sudden emergence of the second optical peak.

7 ACKNOWLEDGEMENTS

REFERENCES

Berger E., Soderberg A.M., Frail D.A., 2003a, GCN 2014
Berger et al. 2003b, astro-ph/0308187
Beuermann et al., 1999, A&A 352, L26
Bikmaev I. et al., 2003, GCN 2220
Bloom J.S., Buxton M., Bailyn C., Van Dokkum P.G., Kulkarni S.R., 2003, GCN 2068
Burenin R. et al., 2003a, GCN 2001
Burenin R. et al., 2003b, Astronomy Lett., Vol. 29, No. 9, 573
Ensman L.M. & Woosley S.E., 1988, ApJ 333, 754
Esin A.A., Blandford R.D., 2000, ApJL, 534, 151
Finkelstein A.M., Ipatov A.V. and Gnedin Y.N., 2003, GCN 2161
Fitzgerald J.B. and Orosz J.A., 2003, GCN 2056
Fox D.W. *et al*, 2003, Nature, 422, 284
Frail D.A. et al., 2001, ApJ 562, L55
Frail D.A. et al., 2003, ApJ 599, 992
Frail D.A., Waxman E. and Kulkarni S.R., 2000, ApJ 537, 191
Galama T.J. et al., 1998, Nature 395, 670
Granot J. & Kumar P., 2003, ApJ 591, 1086
Granot J., Nakar E., Piran T., 2003, astro-ph/0304563
Garnovich P., Matheson T., Olszewski E.W., Harding P. and Stanek K.Z., 2003, IAU Circ. 8114
Greiner J. et al., 2003, GCN 2020
Gorosabel J. et al., 2003, GCN 2242
Harrison F.A. et al., 2001, ApJ 559, 123
Hjorth J. et al., 2003, Nature 423, 847-850
Hoge J.C., Meijerink R., Tilanus R.P.J., Smith I.A., 2003, GCN 2088
Holland S.T., *et al*, 2002, AJ, 124, 639
Holland S.T., *et al*, 2003, AJ, 125, 2291
Ibrahimov M.A. et al., 2003a, GCN 2098
Ibrahimov M.A. et al., 2003b, GCN 2219
Jakobsson P. *et al.* 2003, ApJ, submitted
Kumar P. & Granot J., 2003, ApJ 591, 1075
Kuno N., Sato N. and Nakanishi H., 2003, GNC 2089
Lamb D.Q. et al., 2003, GCN 2040
Lazzati D., Rossi E., Covino S., Ghisellini G., Malesani D., 2003, A&A, 396, 5
Lee B.C., Lamb D.Q., Tucker D.L. and Kent S. on behalf of SDSS GRB team, 2003, GCN 2096
Marshall F.E. and Swank J.H., 2003, GCN 1996
Marshall F.E., Markwardt C. and Swank J.H., 2003, GCN 2052
Matheson T. et al., 2003, astro-ph/0307435

Mèszàros P., 2002, ARA&A40, 137
Nakamura et al., 2001, ApJ 550, 991
Nakar E., Piran T. and Granot J., 2002, ApJ 579, 699
Nakar E., Piran T. and Granot J., 2003, New Astr. 8, 495
Panaitescu A. and Kumar P., 2001a, ApJ 554, 667
Panaitescu A. and Kumar P., 2001b, ApJ 560, L49
Panaitescu A. and Kumar P., 2002, ApJ 571, 779
Panaitescu A. and Kumar P., 2003, ApJ 592, 390
Price A. et al., 2003, Nature 423, 844
Pooley G., 2003a, GCN 2043
Pooley G., 2003b, GCN 2072
Price A., 2003, GCN 2058
Price A. and Mattei J., 2003, GCN 2071
Price A. et al., 2003, GCN 2104
Price A. et al., 2003, GCN 2156
Rao A.P. et al., 2003a, GCN2073
Rao A.P. et al., 2003b, GCN2268
Reichart D., 2001, ApJ, 554, 643
Rhoads J.E., 1997, ApJ 487, L1
Rhoads J.E., 1999, ApJ 525, 737
Salmonson J.D., 2003, ApJ 592, 1002
Sari R. & Mèszàros P., 2000, ApJ 535, L33
Sari R. & Esin A.A., 2001, ApJ 548, 787
Sari R., Piran T. and Narayan R., 1998, ApJ 497, L17
Sari R., Piran T. and Halpern J.P., 1999, ApJ 519, L17
Sheth, K. et al. 2003, astro-ph/0308188
Simoncelli A. et al. 2003, GCN 2124
Stanek K.Z. et al., 2003a, GCN 2120
Stanek K.Z. et al., 2003b, ApJ 591, L17
Susuki J. et al., 2003, GCN 2116
Testa V. et al., 2003, GCN 2141
Tiengo A., Mereghetti S. and Schartel W., 2003a, GCN 2241
Tiengo A., Mereghetti S. and Schartel W., 2003b, GCN 2285
Tiengo A., Mereghetti S., Ghisellini G., Rossi E., Ghirlanda G. and Schartel N., 2003c, A&A, 409, 983
Trushkin S.A. et al., 2003, GCN 2282
Uemura M. et al., 2003, Nature 423, 843
Vanderspek R., et al., 2003, GCN 1997
Walker M., 1998, MNRAS, 294, 307
Wang X., Loeb A., 2000, ApJ, 535, 788
Waxman E., Draine B.T., 2000, ApJ, 537, 796
Weiler K.W., Panagia N., Montes M.J., Sramek R.A., 2002, ARA&A, 40, 387
Wijers R.A.M.J. & Galama T.J., 1999, ApJ 523, 177
Woosley S.E. & Heger A., 2003, astro-ph/0309165
Yost S.A. et al., 2003, astro-ph/0307056
Zharikov S., Benitez E., Torrealba J., Stepnian J., 2003 GCN 2022